Journal of Applied Fluid Mechanics, Vol. 18, No. 12, pp. 2953-2967, 2025.
Available online at www.jafmonline.net, ISSN 1735-3572, EISSN 1735-3645.
https://doi.org/10.47176/jafm.18.12.3534

Performance Investigation of Savonius Hydrokinetic Rotor with Novel Blades Featuring Surface Square Collars and Rectangular Edge Waves

J. S. Patel, V. Rathod, and V. Patel †

Department of Mechanical Engineering, Sardar Vallabhbhai National Institute of Technology, Surat-395007, Gujarat, India

†*Corresponding Author Email: vkp@med.svnit.ac.in*

ABSTRACT

The current work's objective is to investigate how the Savonius rotor performs in relation to the surface square collars and rectangular waves. The experimental study was carried out for three different blade profiles: conventional semicircular blade, semicircular blade with hollow collars, and semicircular blade with closed collars. The results indicate that the rotor with hollow collars outperforms the rotors other two blade profiles. The rotor's highest coefficient of power with hollow collars is 6.68 % and 13.80 % higher than the semicircular bladed conventional rotor and the rotor with closed collars, respectively. This optimized blade was further investigated for different rectangular waves provided between two consecutive collars on the outer side and the inner side. The investigation reveals that the rotor's highest coefficient of power with 0.11 depth to pitch ratio at the outer edge is 13.36 % and 6.28 % higher than the conventional rotor and rotor with 0 depth to pitch ratio respectively, while the highest coefficient of power achieved for the rotor with 0.22 depth to pitch ratio at the inner edge is 14.98% and 7.78 % higher than the conventional rotor and rotor with 0 depth to pitch ratio, respectively.

Article History

Received March 24, 2025
Revised June 24, 2025
Accepted July 9, 2025
Available online October 6, 2025

Keywords:

Vertical axis hydrokinetic turbine
Water stream turbine
Savonius turbine
Drag force driven turbine
Renewable energy

1. INTRODUCTION

Energy consumption has increased due to various causes, including an expanding global population, industrialization, technological breakthroughs, the popularity of electric cars, and smart city projects. Electricity has mostly been produced using fossil fuels as an energy source. Hydrokinetic turbines are excellent alternative renewable energy sources to lower dependency on fossil fuels, which release greenhouse gases, including carbon monoxide, carbon dioxide, nitrous oxide, and methane (Talukdar et al., 2018).

The hydrokinetic turbine makes it feasible and cost-effective to extract the energy of moving water to produce electricity, even in remote areas (Basumatary et al., 2018). Hydrokinetic turbines can be classified into two groups based on their axis orientation: horizontal-axis and vertical-axis turbines (Hazar et al., 2025). The technical difficulties of blade design, generator placement, and cable connection make a vertical axis turbine more useful in hydroelectric applications than a horizontal axis turbine (Khan et al., 2009). Savonius turbines and Darrieus turbines are two forms of vertical axis turbines. Because of their favorable starting characteristics, ease of manufacturing, setup, and maintenance, and low operating costs, Savonius turbines are becoming more popular than Darrieus turbines despite having a lower power generation capacity and coefficient of power (Sharma & Sharma, 2017).

2. ADVANCEMENT IN SAVONIUS TURBINE

Through experiments, Patel et al. (2017) have optimized the inner space between two blades as an overlap ratio (OR) and the rotor height as an aspect ratio (AR). According to the study's findings, in order to maximize the energy harvested from the water flow, the overlap ratio should be maintained between 0.1 and 0.15, and the aspect ratio should be maintained at 1.8.

The impact of the tapered-bladed turbine was numerically studied by Shashikumar et al. (2021) and found that the conventional turbine outperformed the taper-bladed turbine. The effect of two straight plate deflectors was investigated by Salleh et al. (2022). The study concluded that deflector configuration and position

NOMENCLATURE

A	projected area of turbine rotor
C_t	coefficient of torque
Ct_{max}	maximum coefficient of torque
C_p	coefficient of power
Cp_{max}	maximum coefficient of power
r	radius of the turbine shaft
D	diameter of rotor
D_0	diameter of the end plate of the rotor
d_r	shaft diameter
F_r	Fraud number
h	depth of the rectangular wave
N	numbers of revolutions
P	pitch of the wave provided at the outer edge of the blade
P_{max}	maximum power output of the rotor
P_{in}	input power to the turbine or power available in flowing water
P_{out}	mechanical power output from the turbine rotor [W]
R	radius of the turbine rotor
Re	Reynolds number
S	load cell reading
T	torque available at the turbine rotor shaft
T_{max}	maximum torque output of the rotor
U	tip speed of the turbine rotor
V	free stream velocity of flowing water
W	weight applied on weight pan

GREEK SYMBOLS

μ	dynamic viscosity of the water
ρ	density of water
ω	angular velocity of turbine in
λ	wave length of the wave provided at the outer edge of the blade

ABBREVIATIONS

OR	Overlap Ratio
SIMPLE	Semi-Implicit Method for Pressure Linked Equations
SST	Shear Stress Transport
TSR	Tip Speed Ratio

significantly impact the performance. The impact of the semicircular flow deflector placed at the upstream side of the semicircular rotor is experimentally investigated by Patel R. and Patel (2022). They changed the deflector's position throughout the experiment to maximize the rotor's power output. The position of the circular cylindrical deflector was optimized by Yuwono et al. (2020). The impact of a upstream side porous deflector was studied by Eshagh et al. (2020). According to the study's findings, a rotor with a porous deflector performs better than a solid deflector. Yahya et al. (2021) have studied the impact of numbers of guide vanes of 4, 5, and 6 and their tilt angles of 0º, 20º, 40º, and 60º for the semicircular bladed Savonius wind turbine. Optimum performance was obtained for six-numbers guide vanes with a 60º tilt angle.

The shape of the blade has major effects on the rotor's performance. The impact of arc angle of the blade was illustrate by Driss et al. (2015). The impact of the duel splitter was numerically examined by Patel et al. (2021a). Because of the blade's symmetrical design, 2D transient simulation is employed in the study, along with the SST k-ω model for turbulence and SIMPLE algorithm for pressure velocity coupling. At the entrance, Velocity inlet and at the exit pressure outlet with zero-gauge pressure boundary condition is assign. From the study, they found the optimum position of the top splitter of 105º while the bottom splitter kept fixed. Two distinct blades, such as the SR5050 and SS3345, were employed by Tartuferi et al. (2015). The impact of the inner edge arc extension for different lengths and angles was investigated by Abdelaziz et al. (2022) and found the optimum configuration of the rotor, whose C_p is 13.6 % higher compared to the conventional rotor. Kamoji et al. (2009) have experimentally found that the batch-type rotor performs optimally for 0 overlap ratio, 0.7 aspect ratio, 124º blade arc angle, and 0.2 shape factor. Golecha et al. (2011) and Kailash et al. (2012) further optimized this rotor by adding two straight plate deflectors on the upstream side of the rotor. From the study, they find the position of the deflector for which turbine performs optimally. Patel et al. (2023b) examined the effect of the length of the inner edge extension. During the study, they found that a reduction in extension length reduces the performance. Patel et al. (2023c) performed a numerical evaluation of the effect of the extension ratio for the modified Savonius rotor. From the study, they concluded that the turbine performs optimally for an extension ratio of 0.041. The performance of the conventional rotor, batch-type rotor, and elliptical bladed rotor was numerically analyzed by Kacprzak et al. (2013). From the study, they found that the batch-type rotor outperformed the other two. The shape of the blade was optimized by Banh Duc et al. (2023) by providing multiple curves on the blade. From the study, they obtain wind the configuration of the rotor with a higher coefficient of power and 20% higher rotational speed with improved self-starting behavior.

The modified blade with aerodynamic front and was proposed by Kerikous & Thévenin (2019). Patel and Patel (2023) have found that the sharp edge of the blade should be kept outside to obtain better performance. Patel et al. (2021b) examined the impact of arc radius at the blade's inner edge and discovered an adverse impact on the rotor's performance.

Zhang et al. (2021a) introduced the idea of waves on the blade's leading edge for propeller and Darrieus turbines. Patel and Patel (2023) used this idea to a modified Savonius rotor on the blade's outside edge by varying the pitch depth while maintaining a constant wavelength.

According to Thiyagaraj et al. (2020) investigation on the effect of blade count, two-blade turbines were the most effective. Talukdar et al. (2018) observed that the two-

bladed turbine outperformed three-bladed turbine. That's why a two-bladed rotor is considered in the present study.

Kamoji et al. (2009) have found that the provision of a shaft between two blades reduced the performance of the rotor. That's why there is no shaft is placed between two blades and the only shaft that consider in present investigation is to measure torque output which is placed on the support structure.

Patel et al. (2017) examined the consecuences of an endplate and observed that the circular end plate positively affects performance. The impact of end plate shape was studied by Goodarzi & Salimi (2021) for conventional turbines, while Jeon et al. (2015) investigated the helical blade turbine with differently shaped end plates. Both of them concluded that the Savonius turbine with circular end plate performs superior. Hence, in the present investigation, a circular endplate is used at both ends of the blades.

One prominent conclusion drawn from the literature survey is that the turbine's performance is greatly impacted by the blade's shape. The two-blade rotor operates optimally. The provision of a shaft between two blades reduced the performance. The provision of the end plate and its shape significantly affect the performance, especially rotor with circular end plates perform optimally.

Numerous research have been conducted on the shape of the Savonius turbine's blade; however, the idea of a collars on the blade's returning side has not yet been explored. Also, the provision of rectangular waves on the outer and inner edges of the blade is an area that requires further investigation.

3. Data Reduction

3.1. Input Torque

The hydrodynamic torque imparted by flowing water on the turbine is termed input torque. It can be calculated using Eq. (1) (Amiri et al., 2019).

$$T_{in} = \frac{1}{2}\rho A V^2 R \tag{1}$$

3.2. Output Torque

The actual mechanical torque available at the shaft of the turbine is termed output torque. It can be measured by the rope brake dynamometer. It can be calculated using Eq. (2).

$$T_{out} = (F_1 - F_2)r \tag{2}$$

3.3. Coefficient of torque

The ratio of shaft output torque to input torque of the water flow is termed as coefficient of torque. It can be computed using Eq. (3) (Tata et al. 2024).

$$C_t = \frac{T}{\frac{1}{2}\rho A V^2 R} \tag{3}$$

3.4. Tip speed ratio (TSR)

The ratio of the rotor's tangential velocity to the flow velocity (U) is termed as tip speed ratio. It can be computed by using Eq. (4) (Patel et al. 2018; 2023a).

$$TSR = \frac{U}{V} = \frac{D\omega}{2V} \tag{4}$$

3.5. Input Power

The energy imparted by the flowing water is termed as Input power. Input power can be calculated using Eq. (5) (Patel, V.& Patel, 2022).

$$P_{in} = \frac{1}{2}\rho A V^3 \tag{5}$$

3.6. Output Power

Output power is the actual power generated by the turbine. It can be calculated using Eq. (6) (Ramarajan & Jayavel, 2022).

$$P_{out} = T\omega \tag{6}$$

3.7. Coefficient of Power

The rotor's capacity to convert input power into shaft power is indicated by the coefficient of power. It can be computed using Eq.(7) (Kumar & Saini, 2017; John et al., 2020).

$$C_p = \frac{P_{out}}{P_{in}} = \frac{T\omega}{\frac{1}{2}\rho A V^3} = TSR\, C_t \tag{7}$$

4. Conceptual Discussion

The drag force on the upstream side of the returning blade is decreased by the presence of surface square collars. This enhances the turbine's performance and self-starting capability while lowering the braking torque. The hollow passages allow the water to flow through it. That water flow will cause blade to experience drag force. Which positively affects the rotor's performance. That's why the rotor with hollow collars outperforms the rotor with closed collars. The schematic diagram of the 3D flow pattern for the rotor with the hollow collars is shown in Fig. 1.

The provision of rectangular waves on the blade's outer edge causes delay in flow separation, while in the peak plane, it takes place earlier and bleeding of water through the slot from the high-pressure region to the low-pressure region. Which decreases the drag force and increases the lift force imparted by water on the blade (Zhang et al. 2021a, b). This delay in flow separation causes a decrease in breaking torque on the returning blade, which improves the performance of the rotor (Patel & Patel 2023). However, driving torque due to the advancing blade also decreases because of the delay in flow separation, which negatively affects the performance of the rotor. This delay in flow separation depends on the depth of the waves. The schematic diagram of the 3D flow pattern for the rotor with the hollow collars and waves at outer edge is shown in Fig. 2.

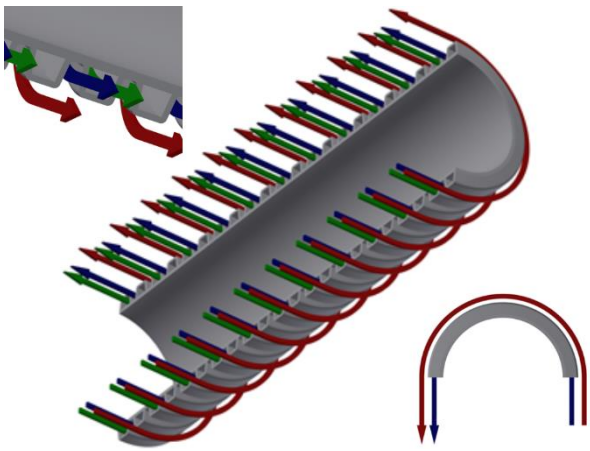

Fig. 1 Schematic of 3D flow pattern for rotor with hollow collars

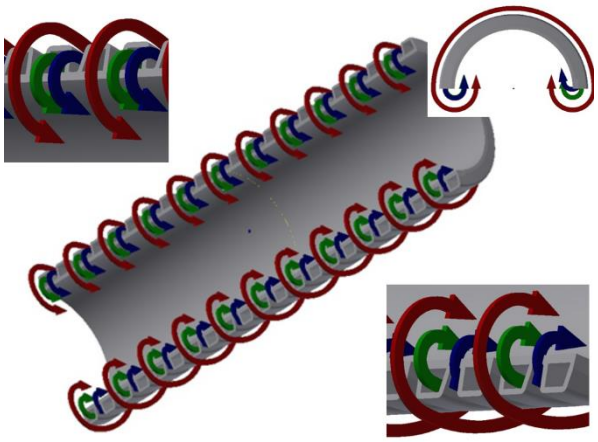

Fig. 2 Schematic of 3D flow pattern for rotor with hollow collars and waves at one edge

The provision of rectangular waves on the inner edge of the blade causes large overlap region, as shown in Fig. 3(b). In the peak plane where the overlap ratio is optimum, flow from the advancing blade strikes on the downstream side of the returning blade, while in the waves region, a larger overlap ratio causes diversion of the flow from the advancing blade. This negatively affects the performance of the rotor as in the waves region, the flow doesn't strike on the downstream side of the returning blade. Also, the provision of the rectangular waves reduces drag force on both blades of the Savonius rotor (Patel & Patel, 2023). The schematic diagram of the 3D flow pattern for the rotor with the hollow collars without waves, inner edge waves, and outer edge waves as shown in Fig. 3.

Both blades feel the force as the flow of water hits the rotor, as Fig. 3 illustrates. A "driving force" force strikes the advancing blade, causing the rotor to rotate; the torque that results is known as "driving torque." Since it prevents the rotor from rotating, the force acting on the returning blade is known as the "breaking force," the torque that results is known as the "breaking torque." Due to their opposing natures, the rotor's net torque production is the difference between the driving and braking torques.

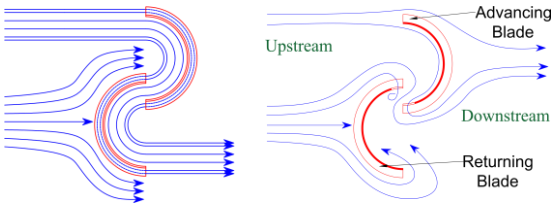

(a) Rotor with hollow collars (b) Rotor with hollow collars and waves at Inner edge

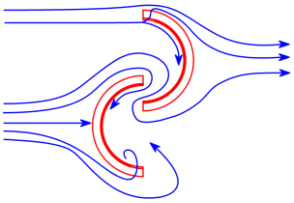

(c) Rotor with hollow collars and waves at Outer edge

Fig. 3 2D flow pattern

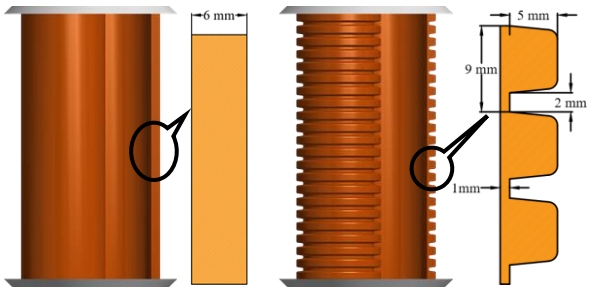

(a) Conventional Rotor (b) Rotor with Closed Collars

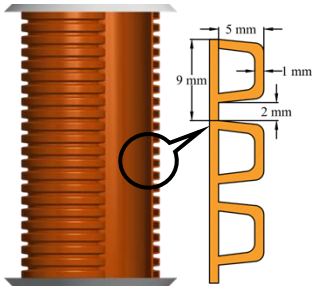

(c) Rotor with Hollow Collars

Fig. 4 Selected blade profile for investigation

5. PARAMETER INVESTIGATED

The goal of this study is to find out how surface square collars impact the Savonius turbine's performance. The study was conducted for three dissimilar blade profiles: conventional semicircular blade, semicircular blade with hollow collars, and semicircular blade with closed collars as shown in Fig. 4.

The optimized blade profile is further optimized by creating rectangular waves at the outer edge of the blade with surface square collars on the returning side. The present study is carried out for the different depth to pitch ratios (h/P) of 0, 0.11, 0.22, 0.33, 0.44, and 0.55 corresponding to different depths of 0, 1, 2, 3, 4, and 5 mm while the pitch of the waves kept constant as shown in Fig. 5.

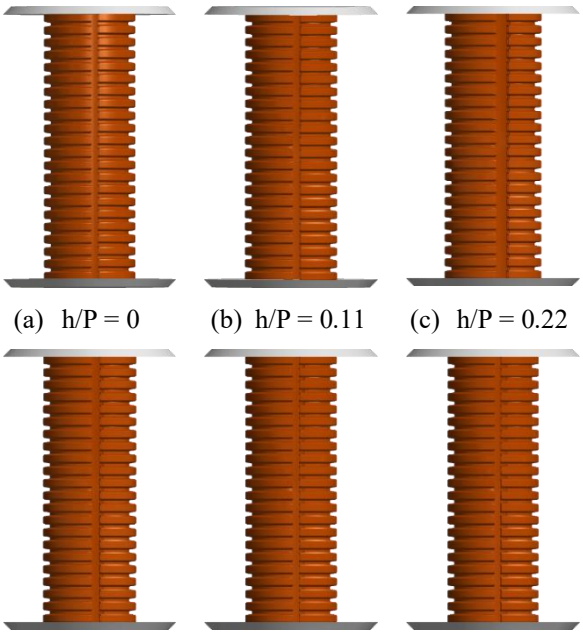

(a) h/P = 0 (b) h/P = 0.11 (c) h/P = 0.22

(d) h/P = 0.33 (e) h/P = 0.44 (f) h/P = 0.56

Fig. 5 Outer waves

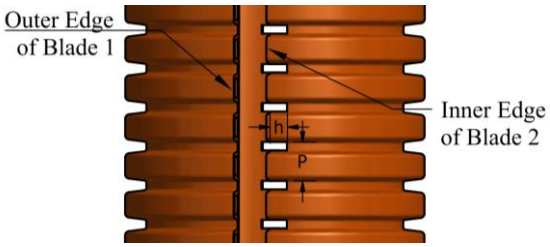

(a) Nomenclature

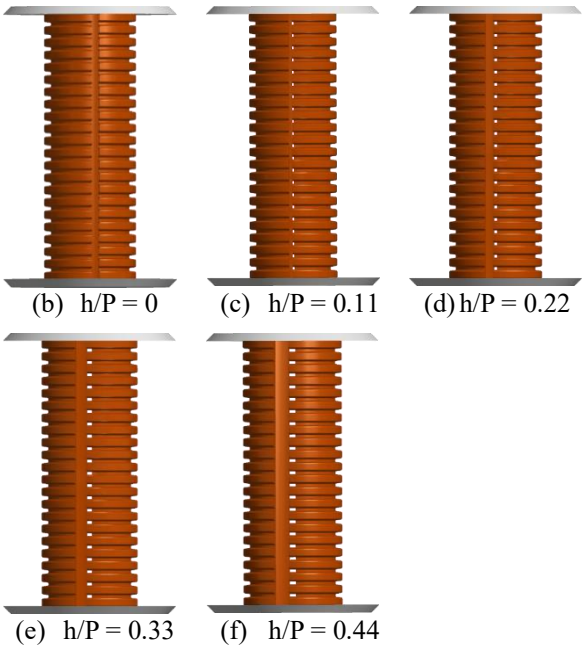

(b) h/P = 0 (c) h/P = 0.11 (d) h/P = 0.22

(e) h/P = 0.33 (f) h/P = 0.44

Fig. 6 Inner waves

This work is further continued by creating rectangular waves at the blade's inner edge with surface square collars on the returning side. The present investigation is conducted for the different depth to pitch ratios (h/P) of 0, 0.11, 0.22, 0.33, and 0.44 corresponding to different depths of 0, 1, 2, 3, and 4 mm while the pitch of the waves kept constant as shown in Fig. 6.

(a) Support structure in canal

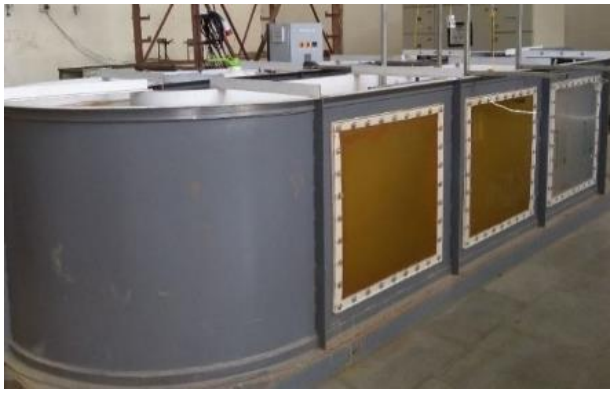

(b) Laboratory canal

Fig. 7 Experimental canal

6. EXPERIMENTAL TECHNIQUES

The present study, the experiments are conducted in a canal with variable frequency drive available at the AFMFP laboratory of S. V. National Institute of Technology, Surat. The experimental procedure in detail is discussed in steps as follows.

6.1. Detail of Experimental Test Facility

The canal is constructed as a continuous unit, which consists of two semicircular sections joined by two straight sections to create an oval shape, as shown in Fig. 7. The submersible pump of 10 Hp is positioned at the center of one straight section whose width is 60 cm and depth of 100 cm. This is followed by the semicircular section equipped with the flow straightener. The purpose of the flow straightener is to reduce the turbulence of the flow so that the flow entering the test section should possess the same characteristics as that of the real canal

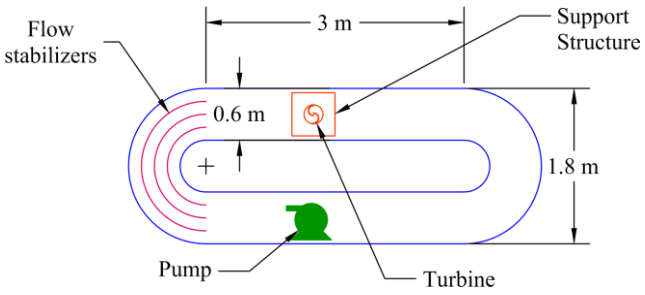

Fig. 8 Laboratory canal schematic

Table 1 Canal Dimensions with specifications

Parameters	Value
Total Canal Length	4.8 m
Width of Flow Section	0.6 m
Total Width of Canal	1.8 m
Depth of Canal	1 m
Water Flow Depth	86 cm
Pump Capacity	10 Hp
Flow Velocity	0.374 m/s

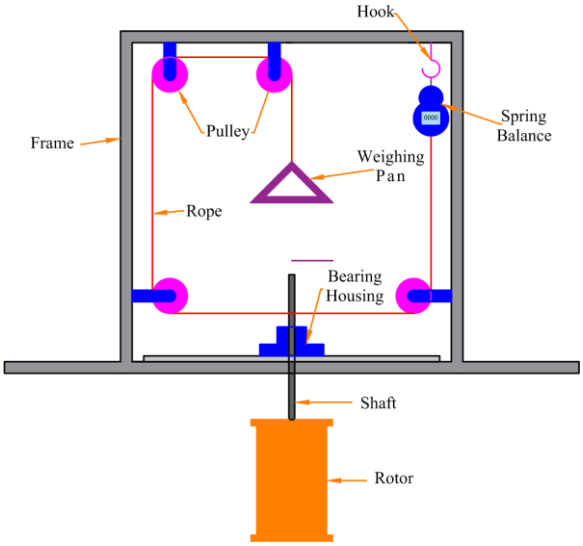

Fig. 9 Schematic diagram of rotor with support structure

flow. The semicircular section with flow straightener is followed by the straight section. The test section is installed at the center of this straight section. The flow of the water in the canal can be controlled by using the variable frequency drive which can operate for the range of 15 Hz to 50 Hz. The specifications of the test facility are as shown in Table 1, while Fig. 8 shows the schematic diagram of the canal.

6.2. Detail of Experimental Setup

The arrangement of the turbine rotor with support structure is shown in Fig. 9. The shaft torque is measured using a rope break type dynamometer. The rope is fastened to the spring balance at one end, while the other end is attached to the weighing pan. The slack side tension in the rope is measured by a spring balance, and the tight side tension is shown by the weighing pan. Bearing housing

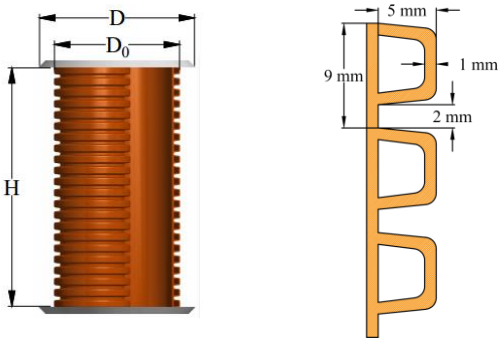

(a) Rotor (b) Cross section of collars

Fig. 10 Rotor used in present study

Table 2 Specification of turbine geometry

Parameters	Values
Diameter of Rotor (*D*)	0.102 m
Pitch (*P*)	0.009 m
Depth to Pitch Ratio (h/P) at Outer Edge	0, 0.11, 0.22, 0.33, 0.44 and 0.55
Depth to Pitch Ratio (h/P) at Inner Edge	0, 0.11, 0.22, 0.33 and 0.44
Height of Rotor (*H*)	0.2 m
Aspect Ratio (AR)	1.96
Shaft Diameter (d_s)	0.01 m
End Plate Ratio (D_0/D)	1.27

and the acrylic plate are used to assemble the rotor on the support structure. The support structure is made flexible so that it can be easily mounted on the canal.

6.3. Turbine Design and Geometry

Table 2 displayed the specifications of the rotor used in the current experimental investigation. Figure 10(a) displays the rotor used in the current study, while Fig. 10(b) displays the cross-section of the collars with dimensions. The blades have a 130 mm circular end plate attached to both ends. The presence of the shaft adversely affects the performance, so no shaft is used between two blades.

6.4. Manufacturing of Rotor Blades and End Plates

The entire turbine setup is fabricated in four parts: two end plates with holes and two blades. The end plate of the rotor is made using a 3D printer of 200 mm x 200 mm bed size, as shown in Fig. 11, while the blades are fabricated from cutting PVC collars pipe. These four parts are assembled with each through the bolts to form the entire setup of the turbine. The blade is prepared by longitudinal cutting of the outer collars-based PVC pipe while PLA (Poly lactic acid) material whose melting point is 190º C to 220º C is used for the fabrication of the end plate. For the proper melting of the filament, the temperature of the nozzle is set as 210 ºC. The bed of the 3D printer was heated to 60 ºC to ensure proper steaking of the printed object with the bed. The filament flow rate is set at 100 %. The 3D printer is set in such a way that the outer edge of the endplate is made with 100 % filling density and the inner portion is made with 50 % filling density.

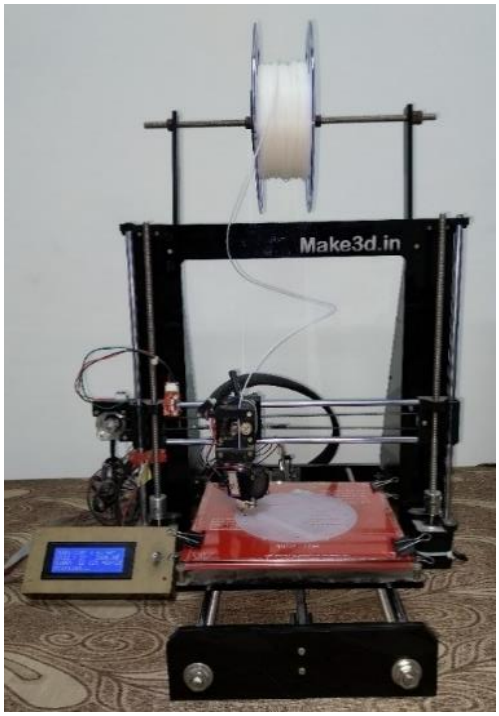

Fig. 11 3D printer

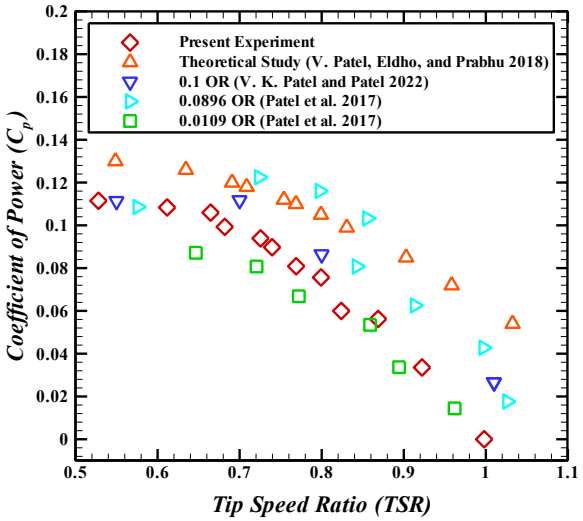

Fig. 12 Comparison of present experimental result with published literature

6.5. Experimental Procedure

First, the laboratory canal was filled with water up to 88 cm of flow depth, which is maintained constant throughout all the experiments. Bolts are used to secure the turbine rotor to the support structure, and the motor frequency is maintained to 40 Hz using a variable frequency drive. A current velocimeter is employed to monitor the flow velocity ten minutes after the pump is started in order to ensure steady-state conditions. The spring balance measures the slack side reaction after applying a known weight to the weight pan. The difference between the spring balance and the weight pan reading shows the effective load on the turbine. Power output is determined using the rotor's torque and rotational velocity, whereas torque is determined using the weight pan and spring balance readings.

6.6. Validation

The present experimental results for the conventional rotor are validated with experimentally obtained and theoretically obtained results for the conventional semicircular rotor, as shown in Fig. 12.

Patel et al. (2018) have prepared a theoretical model for the conventional rotor to predict the coefficient of power based on the principle of impulse-momentum and stagnation pressure concept. Present experiments are carried out for the rotor, whose blades are made out of PVC pipe, and endplates are made in 3D printer using PLA material. Also, the current experimental results are verified with the published experimental findings of the conventional rotor with 0.1 OR (Patel et al., 2018), the conventional rotor with 0.089 OR, and 0.109 OR (Patel et al., 2017) whose rotor is prepared with mounting on the both end plates. Here the entire rotor is submerged in water, and the provision of mounting on both end plates eliminates the possibility of blade deformation. However, in the present study, deformation of the blade is possible specifically at the high load condition, but the close match of the present experimental result and research paper results validate the method used in the current investigation and also show that the effect of the deformation of the blade is negligible.

7. Result and Discussion

The current work's objective is to experimentally investigate how the Savonius rotor performs in relation to the surface square collars and rectangular waves. The experimental study was carried out for three different blade profiles: conventional semicircular blade, semicircular blade with hollow collars, and semicircular blade with closed collars. This optimized blade is further investigated by creating rectangular waves at the outer edge of the blade, and the inner edge of the blade by varying depth and keeping pitch constant. The optimum depth to pitch ratio obtained for the inner edge waves and outer edge waves is considered for the rotor with waves on both edges of the blade.

7.1. Effect of Surface Square Collars

The output torque (shaft torque) is proportional to the effective load (difference between a rope's tight and slack side tensions) applied to it, Whereas the tip speed ratio is proportional to the angular velocity. Initially, for no load condition, the torque output is zero, and the angular velocity is maximum. With an increase in load, torque output increases, and the angular velocity decreases. However, input torque to the rotor remains constant. For this reason, with an increase in the tip speed ratio, the coefficient of torque reduces. The power output of the rotor depends on the shaft torque and the angular velocity. The output torque of the rotor rises with decreases in angular velocity. Initially, for the lower load condition, the impact of an increase in the shaft torque is greater than the decrease in angular velocity.

Consequently, the angular velocity causes the shaft power to rise. After reaching the maximum value, the effect of a drop in the angular velocity becomes apparent

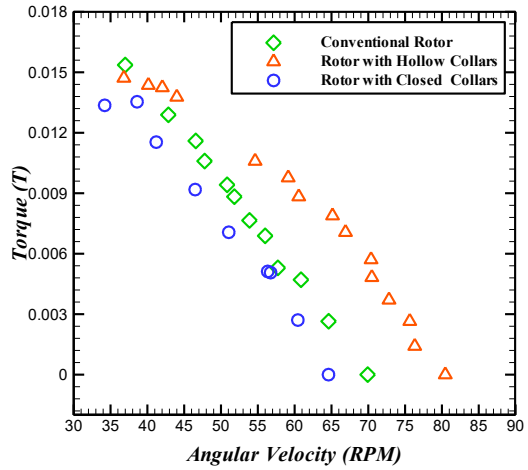

(a) Torque variation with angular velocity

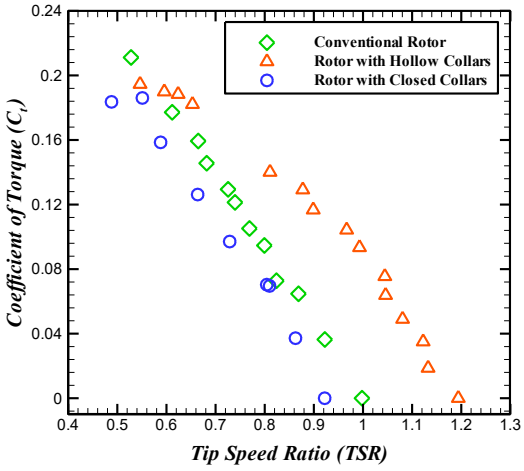

(b) Coefficient of torque variation with TSR

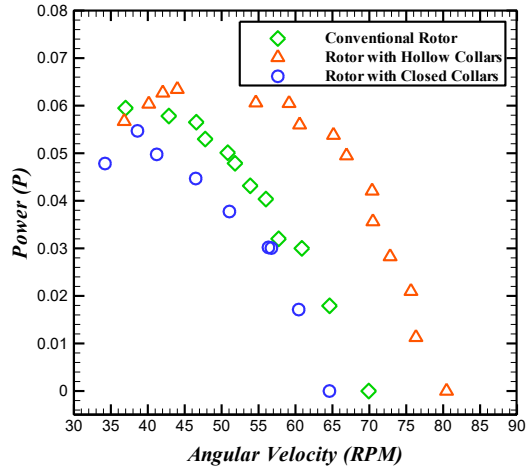

(c) Power variation with angular velocity

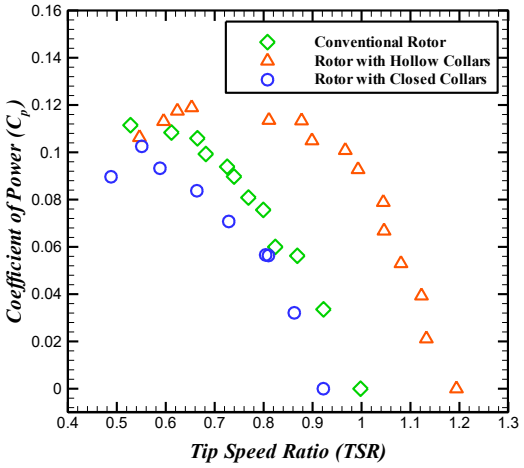

(d) Coefficient of power variation with TSR

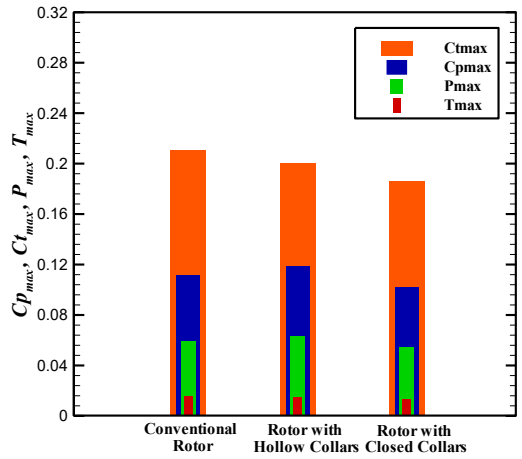

(e) Blade profile performance comparison

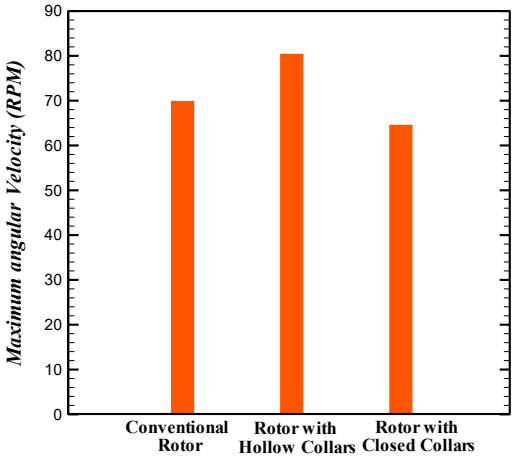

(f) Maximum angular velocity comparison

Fig. 13 Effect of Surface Square Collars

rather than the increase in torque. Therefore, when the angular velocity increases, the shaft power decreases. Because of this, when tip speed ratio increases, so does shaft power. After reaching the maximum value, it decreases as the tip speed ratio rises. However, power input of the flowing water remains constant. As a result, the trend of power variation with angular velocity and coefficient of power variation with the tip speed ratio is identical.

The conventional rotor's torque is higher than other two configurations of the rotor for the angular velocity up to 37 RPM, as shown in Fig. 13(a). However, after 37 RPM, the rotor with hollow collars exhibits higher torque compared to the other two configurations of the rotor. This is because the water flow through the collars imparts drag force on the blade at higher RPM, but at lower RPM, it is ineffective. As a result, the conventional rotor produces

more torque at lower RPMs up to 37, whereas the rotor with hollow collars produces more torque at higher RPMs.

As a result, as seen in Fig. 13, the conventional rotor's power output is higher than that of the rotor with hollow collars up to 37 RPM and the rotor with hollow collars produces more power than the conventional rotor after 37 RPM, as demonstrated in Fig. 13. Here, the rotor's input torque remains constant, and as a result, torque trend and the coefficient of torque's trends follow same pattern. Because of that, the conventional rotor's coefficient of torque is higher than the other two configurations for the tip speed ratio up to 0.55; after 0.55 tip speed ratio, the rotor with hollow collars exhibits higher coefficient torque compared to the other two configurations of the rotor as shown in Fig. 13(b).

The result also demonstrates that the rotor with hollow surface square collars provides a maximum power output of 0.0635 W at 44 RPM and, subsequently a maximum coefficient of power of 0.11892 at 0.653 TSR. Figure 13(e) indicates a relative comparison between three different types of rotor blades. The result indicates that the rotor with a hollow collar improves the maximum coefficient of power by 6.68 % compared to a conventional rotor.

7.2. Effect of Outer Waves

The rectangular waves on the blade's outer edge delay flow separation, while in the peak plane it takes place earlier, and the bleeding of water through the slot decreases the drag force and increases the lift force on the blades. This reduces the breaking torque and improves rotor's performance. This delay in flow separation depends on the depth of the waves. For a small depth to pitch ratio, a delay in flow separation reduces the breaking force on the returning blade; however, an excessive depth to pitch ratio negatively affects the driving torque and performance of the rotor. That's why the torque output initially increases and becomes maximum for 0.11 depth to pitch ratio. After that, it decreases with further increase in depth to pitch ratio, as shown in Fig. 14(a). However, the hydrodynamic torque the flowing water impart does not change. As a result, the coefficient of torque initially increases and becomes maximum for 0.11 depth to pitch ratio. After that, further increase in depth to pitch ratio negatively affects the coefficient of torque, as shown in Fig. 14(b). Initially, with rise in depth to pitch ratio, the rotor's angular velocity increases and becomes maximum at 0.11. Further, increase in depth to pitch ratio negatively affect the rotor's power output. For this reason, the power output rises with an increase in depth to pitch ratio and becomes maximum at 0.11 depth to pitch ratio. Further increase in depth to pitch ratio negatively affects the rotor's power output, as shown in Fig. 14(c). However, input power to the rotor remains constant. For this reason, the rotor's coefficient of power rises as the depth to pitch ratio increases, reaching its maximum at 0.11. Further increase in depth to pitch ratio of the waves negatively affects the rotor's performance, as shown in Fig. 14(d). The comparison of the rotor's maximum performance across all configurations is displayed in Fig. 14(e).

7.3. Effect of Inner Waves

The provision of waves on the inner edge of the blade creates large overlap region. In the peak plane where the overlap ratio is optimum, flow from the upstream side advancing blade strikes on the downstream side of the returning blade, while in the wave region, a larger overlap ratio restricts the flow to strike on the advancing blade. Which reduced the performance of the rotor. Also, the provision of waves on the inner edge of the blade causes delay in flow separation which reduces drag force on both blades. This delay in flow separation is depends on the depth of the waves. For a small depth to pitch ratio, delay in flow separation causes decline in breaking force on the returning blade; however, an excessive depth to pitch ratio negatively affects the driving torque on the rotor. That's why the torque output of the rotor initially increases and becomes maximum for 0.22 depth to pitch ratio. After that, further increase in depth to pitch ratio negatively affects the torque output of the rotor, as shown in Fig. 15(a). However, input torque remains constant. Because of that the coefficient of torque output of the rotor initially increases and becomes highest for 0.22 depth to pitch ratio. After that, further increase in depth to pitch ratio negatively affects the coefficient of torque, as shown in Fig. 15(b). Initially, with an increase in depth to pitch ratio, the angular velocity of the rotor increases and becomes maximum at 0.22. Further, increase in depth to pitch ratio adversely affect the power output. That's why the power output increases with an increase in depth to pitch ratio and becomes maximum at 0.22 depth to pitch ratio. Further increase in depth to pitch ratio negatively affects the power output, as shown in figure 15(c). However, input power to the rotor remains constant. Because of that the coefficient of power follows the same trend as that of the power, as shown in Figure 15(d). Figure 15(e) shows the maximum performance comparison of all configurations of the rotor.

7.4. Effect of Inner Waves and Outer Wave

From the experimental study, the optimum depth to pitch ratio for the rotor with only inner edge waves is 0.22, and for the rotor with only outer edge waves is 0.11. This optimum depth to pitch ratio is considered to form a rotor with waves on both edges of the blade. An experiment is conducted for this rotor arrangement, and its outcomes are compared with the rotor without waves, the rotor with inner waves only with 0.22 depth to pitch ratio, and the rotor with outer waves only with 0.11 depth to pitch ratio as shown in Figure 16. The Savonius rotor's both blades experience less drag force due to the rectangular waves at the blade's edge. Also, the provision of rectangular waves on the inner edge of the blade causes large overlap region, which breaks the overlap jet. As in the waves region, flow does not strike on the downstream side of the returning blade, which reduced the rotor's performance. Therefore, having waves on both sides of the blade has a negative impact on the rotor's performance. Figure 16(e) shows the performance comparison for the four different configurations of the rotor.

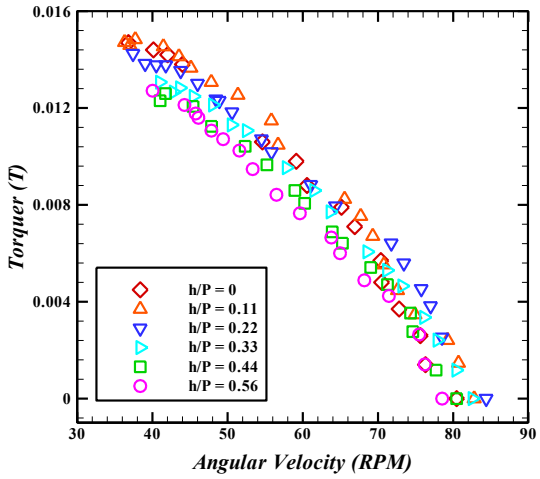

(a) Torque variation with angular velocity

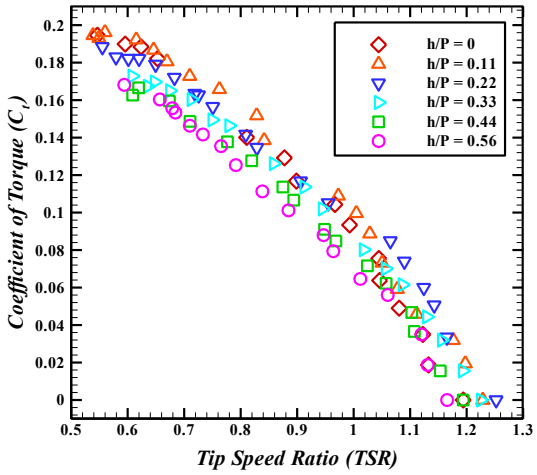

(b) Coefficient of torque variation with TSR

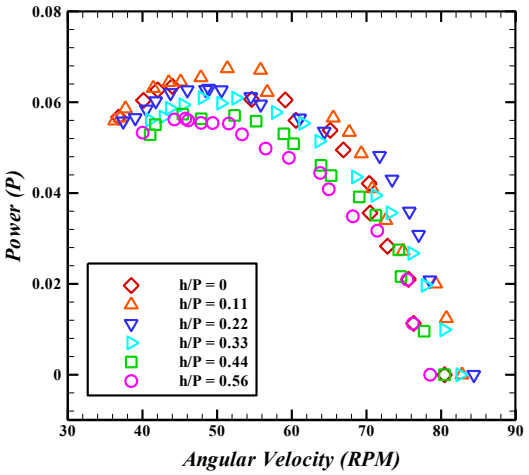

(c) Power variation with angular velocity

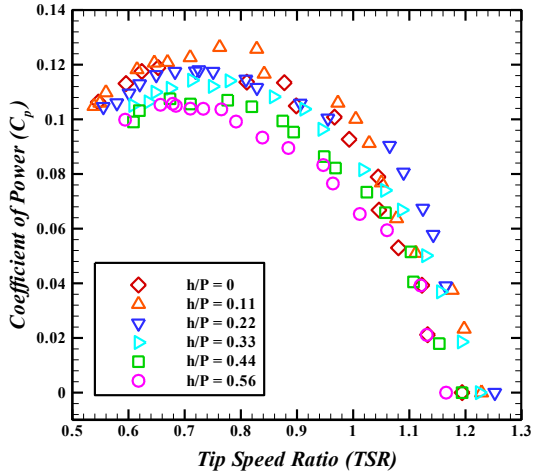

(d) Coefficient of power variation with TSR

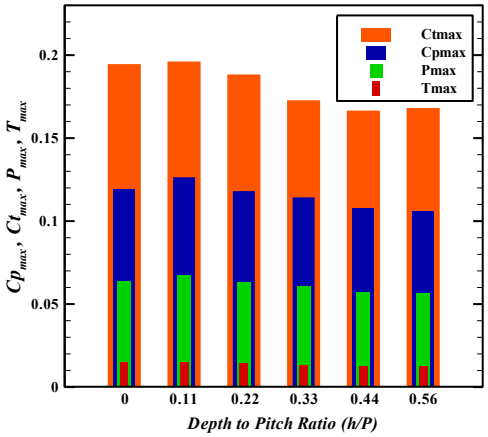

(a) Maximum performance comparison

Fig. 14 Effect of outer waves

8. CONCLUSION

The current experimental work's objective is to investigate how the Savonius rotor performs in relation to the surface square collars and rectangular waves at the outer edge and inner edge of the blade.

Three different rotor's configurations-conventional semicircular rotor, semicircular rotor with hollow collars and semicircular rotor with closed collars was used in current investigations. This optimized rotor is further optimized by providing waves of different depth to pitch ratios (h/P) of 0, 0.11, 0.22, 0.33, 0.44, and 0.56 for the outer edge of the blade and 0, 0.11, 0.22, 0.33, and 0.44 depth to pitch ratio (h/P) for the inner edge. The results of the current investigations lead to the following conclusions:

1. The rotor with hollow collars has maximum C_p that is 6.68 % higher compare to the conventional rotor and

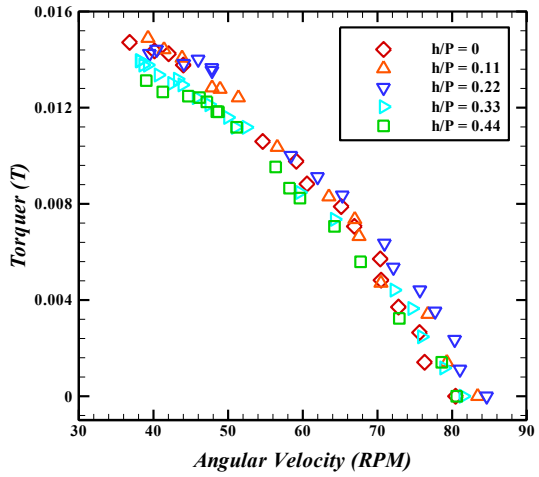

(a) Torque variation with angular velocity

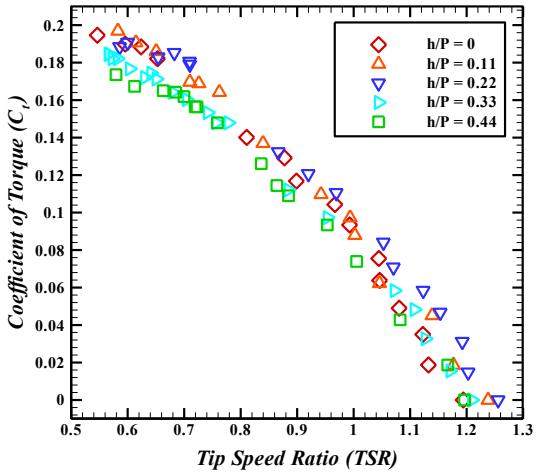

(b) Coefficient of torque variation with TSR

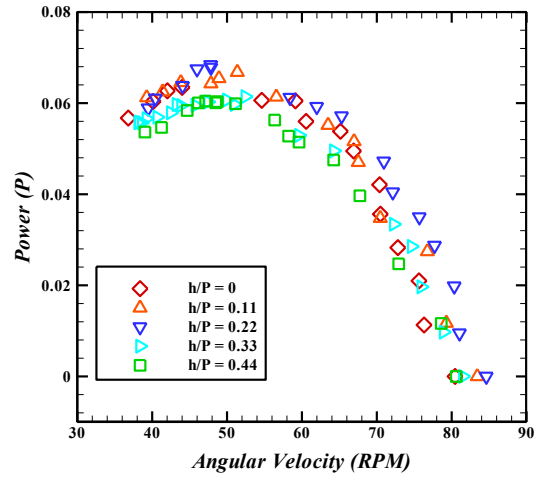

(c) Power variation with angular velocity

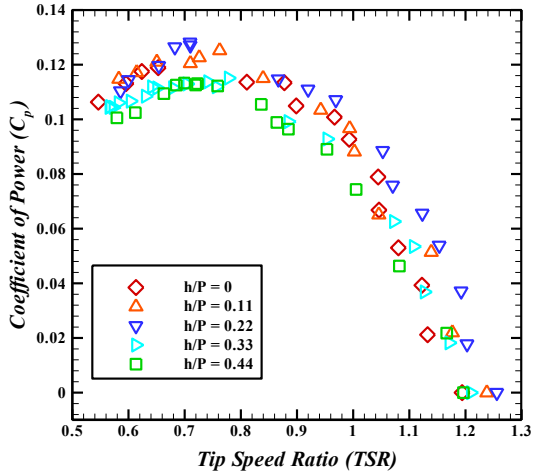

(d) Coefficient of power variation with TSR

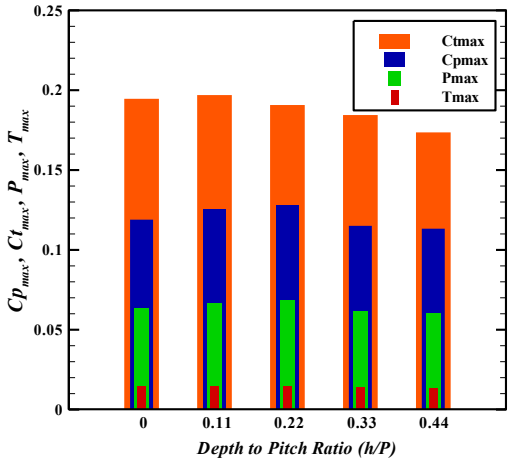

(e) Maximum performance comparison

Fig. 15 Effect of inner waves

13.80 % higher compare to the rotor with closed collars.

2. The rotor with hollow collars' maximum power is 6.68 % higher compare to the conventional rotor and 16.01 % higher compare to the rotor with closed collars.
3. The rotor with hollow collars has a maximum angular velocity that is 15.06 % higher compare to the conventional rotor and 24.54 % higher compare to the rotor with closed collars.
4. For rectangular waves at the outer edge, the maximum C_p of the rotor with 0.11 depth to pitch ratio is 0.1264, which is 13.36 % higher compare to the conventional rotor and 6.28 % higher compare to the rotor with 0 mm depth to pitch ratio.

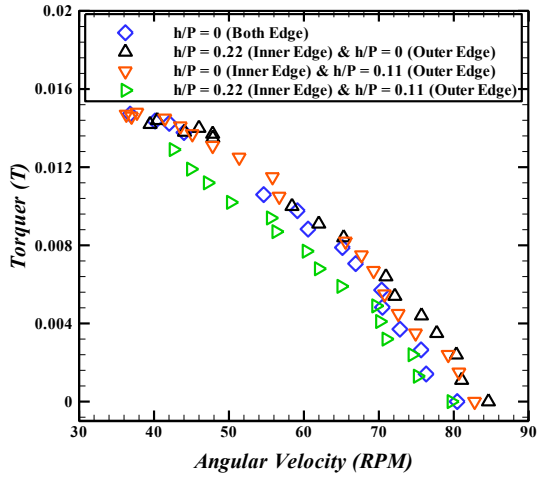

(a) Torque variation with angular velocity

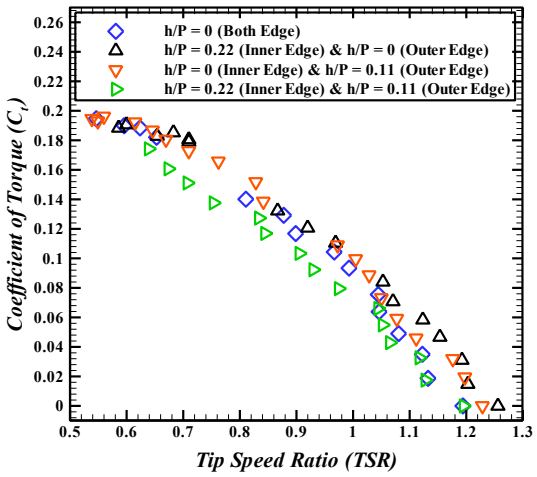

(b) Coefficient of torque variation with tip TSR

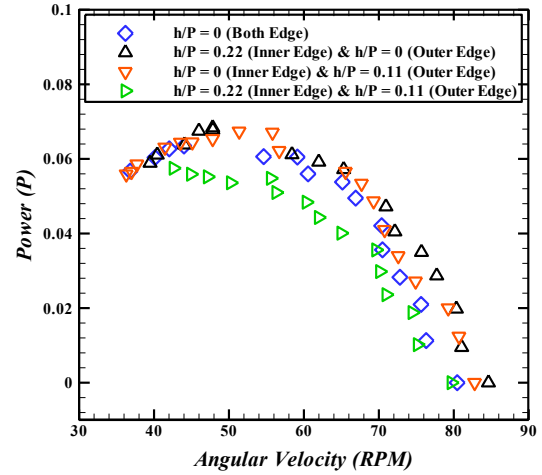

(c) Power variation with angular velocity

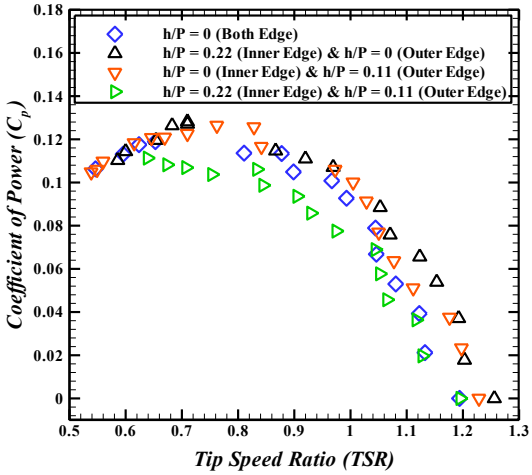

(d) Coefficient of power variation with TSR

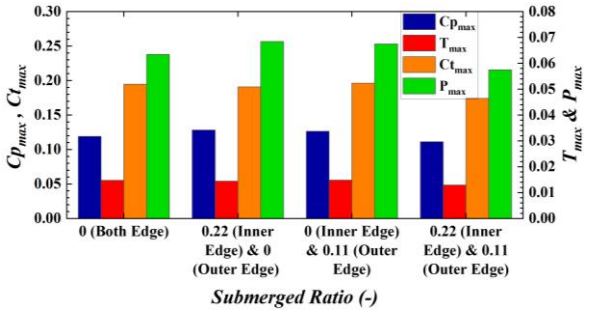

(e) Maximum performance comparison

Fig. 16 Effect of rectangular waves

5. For rectangular waves at the outer edge, the rotor's maximum power output with a 0.11 depth to pitch ratio is 0.0674, which is 11.26 % higher compare to the conventional semicircular rotor and 6.27 % higher compare to the rotor with 0 mm depth to pitch ratio.
6. The maximum C_p of the rotor with 0.22 depth to pitch ratio at the inner edge is 0.1282, which is 14.98 % higher compare to the conventional semicircular rotor and 7.78 % higher compare to the rotor with 0 mm depth to pitch ratio.
7. For rectangular waves at the inner edge, the rotor's maximum power output with 0.22 depth to pitch ratio is 0.0684, which is 12.83 % higher compare to the conventional semicircular rotor and 7.78 % higher compare to the rotor with 0 mm depth to pitch ratio.
8. The provision of rectangular waves on both edges of the blade lowers the performance.

ACKNOWLEDGEMENTS

The work was funded by a core research grant from the Science and Engineering Research Board (SERB), Department of Science and Technology, Delhi, India, for which the authors are extremely grateful. Number of sanction order: CRG/2020/005420.

CONFLICT OF INTEREST

The authors declare that the work presented in this paper could not have been affected by their known competing financial interests or personal relationships.

AUTHORS CONTRIBUTION

Jaykumar S. Patel: Formal assessment, Experimentation, Investigation methodology, Validation, Paper writing, Visualization. **Vimal Patel:** Conceptualization, Formal assessment, Fund securing, Project management, Super- vision, Validation, **Vikram Rathod:** Formal assessment, Fund securing, Project management, Supervision, Validation.

REFERENCES

Abdelaziz, K. R., Nawar, M. A., Ramadan, A., Attai, Y. A., & Mohamed, M. H. (2022). Performance improvement of a savonius turbine by using auxiliary blades. *Energy, 244*, 122575. https://doi.org/10.1016/j.energy.2021.122575

Amiri, M., Kahrom, M., & Teymourtash A. R. (2019). Aerodynamic analysis of a three-bladed pivoted savonius wind turbine: wind tunnel testing and numerical simulation. *Journal of Applied Fluid Mechanics, 12*(3), 819–829. https://doi.org/10.29252/JAFM.12.03.29324

Banh Duc, M., Tran the, H., Dinh Duc, N., Chu Duc, T., & Dinh Le, A. (2023). Performance enhancement of savonius wind turbine by multicurve blade shape. *Energy Sources, Part A: Recovery, Utilization and Environmental Effects, 45*(1), 1624–1642. https://doi.org/10.1080/15567036.2023.2180114

Basumatary, M., Biswas, A., & Misra, R. D. (2018). CFD analysis of an innovative combined lift and drag (CLD) based modified savonius water turbine. *Energy Conversion and Management, 174*, (June): 72–87. https://doi.org/10.1016/j.enconman.2018.08.025

Driss, Z., Mlayeh, O., Driss, S., Driss, D., Maaloul, M., & Abid, M. S. (2015). Study of the bucket design effect on the turbulent flow around unconventional Savonius wind rotors. *Energy, 89*, 708-729. https://doi.org/10.1016/j.energy.2015.06.023

Eshagh, M., Fatahian, H., & Fatahian, E. (2020). Performance improvement of a savonius vertical axis wind turbine using a porous de fl ector. *Energy Conversion and Management*, *220*,(June): 113062. https://doi.org/10.1016/j.enconman.2020.113062

Golecha, K., Eldho, T. I., & Prabhu, S. V. (2011). Influence of the deflector plate on the performance of modified Savonius water turbine. *Applied Energy, 88*(9), 3207-3217. https://doi.org/10.1016/j.apenergy.2011.03.025

Goodarzi, M., & Salimi, S. (2025). Numerical assessment of the effect of different end-plates on the performance of a finite-height Savonius turbine. *Energy Sources, Part A: Recovery, Utilization, and Environmental Effects, 47*(1), 11168-11187. https://doi.org/10.1080/15567036.2021.1976324

Hazar, O., Dirgenali, M., Kaçar, K., & Elçi, S. (2025). Enhancement of savonius wind turbine performance through blade optimization. *Journal of Applied Fluid Mechanics, 18*(5), 1174–1188. https://doi.org/10.47176/jafm.18.5.3177

Jeon, K. S., Jeong, J. I., Pan, J. K., & Ryu, K. W. (2015). Effects of end plates with various shapes and sizes on helical savonius wind turbines. *Renewable Energy, 79*(1), 167–76. https://doi.org/10.1016/j.renene.2014.11.035

John, B., Thomas, R. N., & Varghese, J. (2020). Integration of hydrokinetic turbine-PV-battery standalone system for tropical climate condition. *Renewable Energy, 149*, 361-373. https://doi.org/10.1016/j.renene.2019.12.014

Kacprzak, K., Liskiewicz, G., & Sobczak, K. (2013). Numerical investigation of conventional and modified Savonius wind turbines. *Renewable energy*, *60*, 578-585. https://doi.org/10.1016/j.renene.2013.06.009

Kailash, G., Eldho, T. I., & Prabhu, S. V. (2012). Performance study of modified Savonius water turbine with two deflector plates. *International Journal of Rotating Machinery*, *2012*(1), 679247. https://doi.org/10.1155/2012/679247

Kamoji, M. A., Kedare, S. B., & Prabhu, S. V. (2009). Experimental investigations on single stage modified savonius rotor. *Applied Energy, 86* (7–8), 1064–1073. https://doi.org/10.1016/j.apenergy.2008.09.019

Kerikous, E., & Thévenin, D. (2019). Optimal shape of thick blades for a hydraulic Savonius turbine. *Renewable Energy*, *134*, 629-638. https://doi.org/10.1016/j.renene.2018.11.037

Khan, M. J., Bhuyan, G., Iqbal, M. T., & Quaicoe, J. E. (2009). Hydrokinetic energy conversion systems and assessment of horizontal and vertical axis turbines for river and tidal applications: A technology status review. *Applied Energy, 86*(10), 1823–1835. https://doi.org/10.1016/j.apenergy.2009.02.017

Kumar, A., & Saini, R. P. (2017). performance analysis of a single stage modified savonius hydrokinetic turbine having twisted blades. *Renewable Energy, 113*, 461–78. https://doi.org/10.1016/j.renene.2017.06.020

Patel, C., Rathod, V., & Patel, V. (2023a). Experimental investigations of hydrokinetic turbine providing fillet at the leading edge corner of the runner blades. *Journal of Applied Fluid Mechanics, 16*(4), 865–76. https://doi.org/10.47176/jafm.16.04.1533

Patel, J. S., Patel, V. K., & Rathod, V. P. (2023b). Influence of negative overlap ratio on the performance of semicircular savonius rotor with

straight edge extension on overlap region. *Green Energy and Technology*, 317–330. https://doi.org/10.1007/978-981-99-2279-6_27

Patel, J. S., Rathod, V., & Patel, V. (2023c). Influence of extension ratio on the performance of the modified Savonius hydrokinetic turbine. *Journal of Energy Engineering*, *149*(6), 04023043. https://doi.org/10.1061/JLEED9.EYENG-4992

Patel, R., & Patel, V. (2023). Effect of waves on leading edge of modified Savonius rotor blades. *Ocean Engineering*, *271*, 113445. https://doi.org/10.1016/j.oceaneng.2022.113445

Patel, R., & Patel, V. (2022). Performance analysis of Savonius hydrokinetic turbine using 'C'shaped Deflector. *Energy Sources, Part A: Recovery, Utilization, and Environmental Effects*, *44*(3), 6618-6631. https://doi.org/10.1080/15567036.2022.2101718

Patel, V. K., & Patel, R. S. (2022). Optimization of an angle between the deflector plates and its orientation to enhance the energy efficiency of Savonius hydrokinetic turbine for dual rotor configuration. *International Journal of Green Energy*, *19*(5), 476-489. https://doi.org/10.1080/15435075.2021.1947821

Patel, V., & Patel, R. (2021a). Free energy-extraction using Savonius hydrokinetic rotor with dual splitters. *Materials Today: Proceedings*, *45*, 5354-5361. https://doi.org/10.1016/j.matpr.2021.01.928

Patel, V., & Patel, R. (2021b). Energy extraction using modified Savonius rotor from Free-flowing water. *Materials Today: Proceedings*, *45*, 5190-5196. https://doi.org/10.1016/j.matpr.2021.01.703

Patel, V., Bhat, G., Eldho, T. I., & Prabhu, S. V. (2017). Influence of overlap ratio and aspect ratio on the performance of Savonius hydrokinetic turbine. *International Journal of Energy Research*, *41*(6), 829-844. https://doi.org/10.1002/er.3670

Patel, V., Eldho, T. I., & Prabhu, S. V. (2018). Theoretical study on the prediction of the hydrodynamic performance of a Savonius turbine based on stagnation pressure and impulse momentum principle. *Energy Conversion and Management*, *168*, 545-563. https://doi.org/10.1016/j.enconman.2018.04.065

Ramarajan, J., & Jayavel, S. (2022). Performance Improvement in Savonius Wind Turbine by Modification of Blade Shape. *Journal of Applied Fluid Mechanics,* *15*(1), 99–107. https://doi.org/10.47176/jafm.15.01.32516

Salleh, M. B., Kamaruddin, N. M., & Mohamed-Kassim, Z. (2022). Experimental investigation on the effects of deflector angles on the power performance of a Savonius turbine for hydrokinetic applications in small rivers. *Energy*, *247*, 123432. https://doi.org/10.1016/j.energy.2022.123432

Sharma, S., & Sharma, R. K. (2017). CFD investigation to quantify the effect of layered multiple miniature blades on the performance of Savonius rotor. *Energy Conversion and Management, 144*, 275–285. https://doi.org/10.1016/j.enconman.2017.04.059

Shashikumar, C. M., Vijaykumar, H., & Vasudeva, M. (2021). Numerical investigation of conventional and tapered Savonius hydrokinetic turbines for low-velocity hydropower application in an irrigation channel. *Sustainable Energy Technologies and Assessments*, *43*, 100871. https://doi.org/10.1016/j.seta.2020.100871

Talukdar, P. K., Sardar, A., Kulkarni, V., & Saha, U. K. (2018). Parametric analysis of model Savonius hydrokinetic turbines through experimental and computational investigations. *Energy Conversion and Management*, *158*, 36-49. https://doi.org/10.1016/j.enconman.2017.12.011

Tartuferi, M., D'Alessandro, V., Montelpare, S., & Ricci, R. (2015). Enhancement of savonius wind rotor aerodynamic performance: a computational study of new blade shapes and curtain systems. *Energy, 79,* 371-384. https://doi.org/10.1016/j.energy.2014.11.023

Tata, M., Bekhti, A., Maizi, M., Cherifi, N. O., Tamoum, A., Hamane, D., Boudis, A., Debbache, M., & Guerri, O. (2024). Aerodynamic performance investigations of savonius twin-rotor wind turbines. *Journal of Applied Fluid Mechanics, 17*(2), 442–460. https://doi.org/10.47176/jafm.17.02.2044

Thiyagaraj, J., Rahamathullah, I., Anbuchezhiyan, G., Barathiraja, R., & Ponshanmugakumar, A. (2020). Influence of blade numbers, overlap ratio and modified blades on performance characteristics of the savonius hydro-kinetic turbine. *Materials Today: Proceedings, 46*, 4047–53. https://doi.org/10.1016/j.matpr.2021.02.568

Yahya, W., Ziming, K., Juan, W., Qurashi, M. S., Al-Nehari, M., & Salim, E. (2021). Influence of tilt angle and the number of guide vane blades towards the Savonius rotor performance. *Energy Reports*, *7*, 3317-3327. https://doi.org/10.1016/j.egyr.2021.05.053

Yuwono, T., Sakti, G., Aulia, F. N., & Wijaya, A. C. (2020). Improving the performance of Savonius wind turbine by installation of a circular cylinder upstream of returning turbine blade. *Alexandria Engineering Journal*, *59*(6), 4923-4932. https://doi.org/10.1016/j.aej.2020.09.009

Zhang, Y. N., Cao, H. J., & Zhang, M. M. (2021a). Investigation of leading-edge protu berances for the performance improvement of thick wind turbine airfoil1. *Journal of Wind Engineering and Industrial Aerodynamics*, *217*, 104736. https://doi.org/10.1016/j.jweia.2021.104736.

Zhang, Y., Zhang, X., Chang, M., & Xu, J. (2021b). Aerodynamic performance of a low-Reynolds UAV with leading-edge protuberances inspired by

humpback whale flippers. *Chinese Journal of Aeronautics*, *34*(5), 415-424. https://doi.org/10.1016/j.cja.2020.11.004

ANNEXURE A: UNCERTAINTY ANALYSIS

Uncertainty associated with present experimental results of the conventional semi-circular blade rotor is calculated by using following equation.

$$\frac{dC_p}{C_p}=\sqrt{\left(\frac{dF}{F}\right)^2+\left(\frac{dd}{d}\right)^2+\left(\frac{d\omega}{\omega}\right)^2+\left(\frac{dD}{D}\right)^2+\left(\frac{dH}{H}\right)^2+3\left(\frac{dV}{V}\right)^2}$$

Table A1 Uncertainty Analysis conventional semi-circular blade rotor

Torque (Nm)	$\frac{dT}{T}$ (%)	ω (rad/s)	TSR (-)	C_p (-)	$\frac{dC_p}{C_p}$ (%)
0.00265	1.5745	6.7634	0.9223	0.03357	1.6479
0.0053	0.7920	6.0415	0.8238	0.05998	0.9323
0.00471	0.8895	6.3708	0.8687	0.05622	1.0151
0.00765	0.5530	5.6389	0.7690	0.08086	0.7429
0.00689	0.6126	5.8612	0.7993	0.07564	0.7867
0.00942	0.4531	5.3202	0.7255	0.09390	0.6747
0.00883	0.4819	5.4236	0.7396	0.08974	0.6934
0.0116	0.3726	4.8745	0.6647	0.10593	0.6289
0.0106	0.4054	5.0006	0.6819	0.09928	0.6472
0.01289	0.3380	4.4856	0.6117	0.10836	0.6153
0.01536	0.2888	3.8719	0.5280	0.11147	0.6039

$$\text{Where } dF=\sqrt{(dW)^2+(dS)^2}$$

Standard weight us used on the tight side of the dynamometer with uncertainty of 0.5 gm, slack side readings are measured with spring balance with measurement uncertainty of 0.5 gm. Rotor dimeter, height, shaft diameter measured with digital Vernier calliper with least count of 0.01 mm and velocity current meter is used to measure the free stream velocity of the flow with uncertainty of 0.001 m/s. Table shows the value of the uncertainty associated with torque coefficient of power calculated by using above equations.

ANNEXURE B: PERFORMANCE DATA

Table B1 Performance comparison of three different rotors

Rotor	T_{max}	P_{max}	Ct_{max}	Cp_{max}
Conventional	0.0154	0.0595	0.2111	0.1115
Rotor with hollow collar	0.0152	0.0635	0.2008	0.1189
Rotor with Closed collar	0.0135	0.0547	0.1861	0.1025

Table B2: Performance comparison for outer edge wave

h/P	T_{max}	P_{max}	Ct_{max}	Cp_{max}
0	0.014715	0.063457	0.194599	0.118923
0.11	0.014833	0.067443	0.196156	0.126393
0.22	0.014244	0.062994	0.188372	0.118056
0.33	0.013067	0.060996	0.172804	0.114312
0.44	0.012596	0.057377	0.166577	0.107529
0.56	0.012714	0.056398	0.168134	0.105693

Table B3 Performance comparison for inner edge wave

h/P	T	P	Ct	Cp
0	0.014715	0.063457	0.194599	0.118923
0.11	0.014892	0.06681	0.196934	0.125206
0.22	0.014421	0.068394	0.190707	0.128175
0.33	0.01395	0.061423	0.18448	0.11511
0.44	0.013126	0.060451	0.173582	0.11329